

# Diabetes-Impaired Wound Healing Is Improved by Matrix Therapy With Heparan Sulfate Glycosaminoglycan Mimetic OTR4120 in Rats

Miao Tong,<sup>1</sup> Bastiaan Tuk,<sup>1</sup> Peng Shang,<sup>2</sup> Ineke M. Hekking,<sup>1</sup> Esther M.G. Fijneman,<sup>1</sup> Marnix Guijt,<sup>1</sup> Steven E.R. Hovius,<sup>1</sup> and Johan W. van Neck<sup>1</sup>

Wound healing in diabetes is frequently impaired and its treatment remains a challenge. We tested a therapeutic strategy of potentiating intrinsic tissue regeneration by restoring the wound cellular environment using a heparan sulfate glycosaminoglycan mimetic, OTR4120. The effect of OTR4120 on healing of diabetic ulcers was investigated. Experimental diabetes was induced by intraperitoneal injection of streptozotocin. Seven weeks after induction of diabetes, rats were ulcerated by clamping a pair of magnet disks on the dorsal skin for 16 h. After magnet removal, OTR4120 was administered via an intramuscular injection weekly for up to 4 weeks. To examine the effect of OTR4120 treatment on wound healing, the degree of ulceration, inflammation, angiogenesis, and collagen synthesis were evaluated. We found that OTR4120 treatment significantly reduced the degree of ulceration and the time of healing. These effects were associated with reduced neutrophil infiltration and macrophage accumulation and enhanced angiogenesis. OTR4120 treatment also increased the collagen content with an increase of collagen type I biosynthesis and reduction of collagen type III biosynthesis. Moreover, restoration of the ulcer biomechanical strength was significantly enhanced after OTR4120 treatment. This study shows that matrix therapy with OTR4120 improves diabetes-impaired wound healing.

**I**mpaired wound healing is a well-documented phenomenon both in experimental and clinical diabetes (1). Several mechanisms for diabetes-impaired wound healing are proposed that are mostly related to impairment of macrophage function (2), angiogenic response (3), and extracellular matrix (ECM) deposition (4). The ideal treatment relies on correcting the multiple deficits simultaneously through highly integrated and personalized therapeutic approaches.

Wound healing is associated with dynamic interactions between the ECM and growth factors (GFs) (5). The ECM consists of a network of scaffold proteins that are bridged by glycosaminoglycans (GAGs), of which heparan sulfate (HS) is an important component. HS-GAGs are capable of transmitting signals by providing binding sites for a large variety of HS-bound signaling peptides (i.e., GFs, chemokines, and cytokines). However, after tissue injury, the glycanases and proteases can destroy HS-GAGs (6). As

a result, the ECM-GF interactions are disturbed. These disruptions characterize impaired wounds (5,7) and also may have the implication of matrix therapy.

OTR4120 is an HS-GAG mimetic that can replace the degraded HS-GAGs and protect and improve the bioavailability of GFs, cytokines, and other heparin-binding signaling peptides. In this way, OTR4120 offers a matrix therapy that restores the natural cellular microenvironment and the endogenous signaling of cell communications needed for tissue regeneration (8–10). This facilitates the quality of healing by potentiating the intrinsic tissue regeneration.

The current study evaluates the efficacy of matrix therapy with OTR4120 in pressure ulcers generated in streptozotocin (STZ)-induced diabetic rats.

## RESEARCH DESIGN AND METHODS

**Animals.** WAG/RijHsd female rats (142, 10 weeks old) were purchased from Harlan (Zeist, the Netherlands). Rats were exposed to a 12-h light-dark cycle and fed a standard laboratory diet with food and water available ad libitum. All procedures with animals were approved by the local Animal Experiments Committee.

**Induction of diabetes.** After overnight fasting, animals were given an intraperitoneal injection of STZ (Sigma-Aldrich, St. Louis, MO) at a dose of 65 mg/kg body weight in 0.05 mol/L sodium citrate buffer, pH 4.5. Blood glucose concentration was monitored weekly by a OneTouch glucometer (LifeScan, Milpitas, CA) from tail vein blood. A prolonged diabetes status was defined as blood glucose levels  $\geq 20$  mmol/L throughout the induction period.

**Ulceration model and OTR4120 treatment.** Seven weeks after STZ injection, 119 diabetic rats were obtained and ulcerated by clamping and then removal of a pair of magnet disks (15-mm diameter) on rat dorsal skin for a single ischemic period of 16 h. After wounding, rats were randomly allocated to six groups to serve six experimental end points (i.e., day 3,  $n = 16$ ; day 7,  $n = 18$ ; day 14,  $n = 18$ ; day 18,  $n = 15$ ; day 42,  $n = 34$ ; and day 84,  $n = 18$ ). Lyophilized OTR4120 was rehydrated in a physiological salt solution (B. Braun Melsungen AG, Melsungen, Germany) at a concentration of 1 mg/mL. Immediately after magnet removal, rats were randomly assigned to receive an intramuscular injection of OTR4120 in the thigh at a dose of 1 mg/kg body weight or the same volume of physiological salt solution weekly for up to 1 month. The OTR4120 dosage was based on the experience from the previous studies (11–15). At each experimental end point, the animals were killed simultaneously. The experiment was blinded to all observers.

**Macroscopic analysis.** Body weight and blood glucose levels were measured and the ulcers were photographed. The ulcers were graded according to the grading system of the National Pressure Ulcer Advisory Panel (16). The percentage of completely closed ulcers was calculated.

**Immunohistochemistry.** Paraffin-embedded sections (5  $\mu$ m) were deparaffinized and rehydrated. Antigen retrieval was performed in Tris-EDTA (TE) buffer containing 0.1% trypsin (Invitrogen, Carlsbad, CA). Endogenous peroxidase activity was quenched by exposing to 0.1% hydrogen peroxide in PBS containing 0.1% Tween 20 (PBST). After blocking with 4% nonfat milk powder in PBST, the sections were incubated with mouse anti-CD68 (1:100; AbD Serotec, Düsseldorf, Germany) and goat anti-CD34 (1:200; R&D Systems, Minneapolis, MN), respectively, followed by incubating with the corresponding biotinylated secondary antibodies (R&D Systems). The antigen-antibody complex was detected by streptavidin-peroxidase (R&D Systems) and 3,3'-diaminobenzidine (Dako, Carpinteria, CA). For evaluation of staining, the

From the <sup>1</sup>Department of Plastic and Reconstructive Surgery, Erasmus MC, University Medical Center, Rotterdam, the Netherlands; and the <sup>2</sup>Department of Reproduction and Development, Erasmus MC, University Medical Center, Rotterdam, the Netherlands.

Corresponding author: Miao Tong, m.tong@hotmail.com.

Received 6 October 2011 and accepted 23 April 2012.

DOI: 10.2337/db11-1329

© 2012 by the American Diabetes Association. Readers may use this article as long as the work is properly cited, the use is educational and not for profit, and the work is not altered. See <http://creativecommons.org/licenses/by-nc-nd/3.0/> for details.

overview of the positive-signal density was scored semiquantitatively as 1 (absent), 2 (low), 3 (medium), 4 (strong), and 5 (very strong). The median of scores from three observers, who were blinded to the treatment, was used for comparisons.

**Myeloperoxidase assay.** Myeloperoxidase (MPO) activity in ulcer tissue homogenates was assayed as previously described with minor modifications (17). In brief, homogenates were mixed in 100 mmol/L sodium acetate buffer containing 0.5% hexadecyl trimethyl ammonium bromide (Sigma-Aldrich, St. Louis, MO). The mixture was centrifuged to extract the MPO. After centrifugation, the supernatant was incubated at 37°C for 15 min in 100 mmol/L sodium acetate buffer, containing 0.0005% hydrogen peroxide, 3.2 mmol/L 3,3',5,5'-tetramethylbenzidine dihydrochloride (Sigma-Aldrich), and 0.5% hexadecyl trimethyl ammonium bromide. The optical densities were recorded at 660 nm. MPO content was determined as units per gram tissue homogenate by using a standard curve generated by purified MPO from human leukocytes (Sigma-Aldrich).

**Western blot analysis.** Protein contents of vascular endothelial growth factor (VEGF), platelet-derived growth factor (PDGF), transforming growth factor- $\beta$ 1 (TGF- $\beta$ 1), and inducible nitric oxide synthase (iNOS) in ulcer tissue homogenates were evaluated by Western blot as described previously (11). In brief, the protein concentrations of homogenates were determined using RxDc Protein Assay Kit (Bio-Rad, Hercules, CA). An equivalent amount of protein was separated on an SDS polyacrylamide gel and transferred onto a polyvinylidene difluoride membrane (Bio-Rad). Blocking was performed in 3% BSA (Sigma-Aldrich) in 10 mmol/L Tris and 150 mmol/L NaCl, containing 0.1% Tween-20. The membranes were probed with 1:1,000 diluted mouse anti-VEGF (Santa Cruz Biotechnology, Santa Cruz, CA), 1:400 diluted rabbit anti-PDGF (Santa Cruz Biotechnology), 1:500 diluted mouse anti-TGF- $\beta$ 1 (R&D Systems), and 1:400 diluted rabbit anti-iNOS (Calbiochem, San Diego, CA), respectively. Binding of the primary antibody was detected using a peroxidase-conjugated secondary antibody (Pierce, Rockford, IL). Positive bands were visualized using chemiluminescence (Supersignal; Pierce).

**Hydroxyproline content and collagen type I and type III ex vivo biosynthesis measurements.** Ulcer biopsies were labeled with 50 mCi [ $^3$ H]hydroxyproline (GE Healthcare, Diegem, Belgium) for 24 h in Dulbecco's modified Eagle's minimal essential medium supplemented with 100 IU/mL penicillin, 100 mg/mL streptomycin, and 2 mmol/L glutamine. The tissue was then washed extensively until no radioactivity was detected. Subsequently, the labeled biopsies were homogenized, and a small aliquot of the homogenates was hydrolyzed in 6 N HCl at 100°C for 24 h. The total collagen content was determined by colorimetric hydroxyproline assay (18). All remaining homogenates were digested with 1% pepsin (Sigma-Aldrich) in 0.5 M acetic acid for 48 h. After centrifugation, the supernatant was dialyzed against 0.5 M acetic acid for 24 h and then lyophilized. Before lyophilization, the total pepsin-soluble biosynthesized collagen was measured by determining the amount of [ $^3$ H]hydroxyproline in the dialysates. Biosynthesis of collagen type I and III was determined after electrophoresis of a 1-mg lyophilized sample on SDS-PAGE. The collagen bands were revealed by Coomassie Brilliant Blue staining and identified by comparison with standard collagen type I and type III. The relative proportions of radioactivity incorporated in collagen types were quantified by excision of each individual collagen band followed by hydrolysis

of the band in 6 N HCl at 100°C for 24 h, after which [ $^3$ H]hydroxyproline was determined in the hydrolysate (12).

**Breaking strength measurement.** Breaking strength was measured as described previously (13). In brief, the excised dorsal pelt, containing an ulcer, was cut into two standardized dumbbell-shaped skin strips. One strip was centered by a segment of ulcer, and the other was cut from the surrounding normal skin. The strip was fixed perpendicularly between the two clips of a tensiometer and subjected to a constant strain rate of 60 mm/min using a 1.0-kg force transducer. Breaking strength was recorded as the maximum load (Newton) measured before skin failure. The ratio of ulcer breaking strength to that of surrounding normal skin breaking strength was calculated for data analysis.

## REAL-TIME QUANTITATIVE PCR

Total RNA from tissues was isolated using TRIzol reagent (Invitrogen). Five micrograms of total RNA was treated for 15 min with DNase I prior to a 50-min reverse transcription reaction using a SuperScript II RT Kit (Invitrogen). Quantitative PCR was performed with a SYBR Green PCR Master Mix (Applied Biosystems, Carlsbad, CA) using a C1000 thermal cycler (Bio-Rad). Melting curves were used as quality controls to exclude samples with genomic DNA content and to ensure single product amplification.  $\beta$ -Actin levels were used for internal normalization. Data were analyzed with the CFX Manager 2.1 software package (Bio-Rad). The primer sets are described as follows: VEGF-A, forward 5'-ACGTCACTATGCAGATCATGC-3' and reverse 5'-CCTTTCCCTTT-CCTCGAACTG-3'; TGF- $\beta$ 1, forward 5'-CAATTCCTGGCGT-TACCTTG-3' and reverse 5'-AAAGCCCTGTATTCCGTCTC-3'; and iNOS, forward 5'-GAACTCGGGCATACTTCAG-3' and reverse 5'-CTCCCAGGTGAGACAGTTTC-3'.

**Statistical analysis.** Data are presented as means  $\pm$  SEM. Statistical calculations were performed using SPSS software, version 11 (Chicago, IL). The Mann-Whitney *U* test was carried out to compare results between groups. A *P* value  $\leq 0.05$  was considered to indicate a statistically significant difference.

## RESULTS

**Diabetes induction.** During the 7-week diabetes induction period, 84% of the STZ-injected rats became consistently hyperglycemic and were included in this study. Of the STZ-injected rats, 7% had glucose levels  $\leq 20$  mmol/L, 5% died, and 4% were killed because of a body weight loss of  $\geq 10$  g/week.

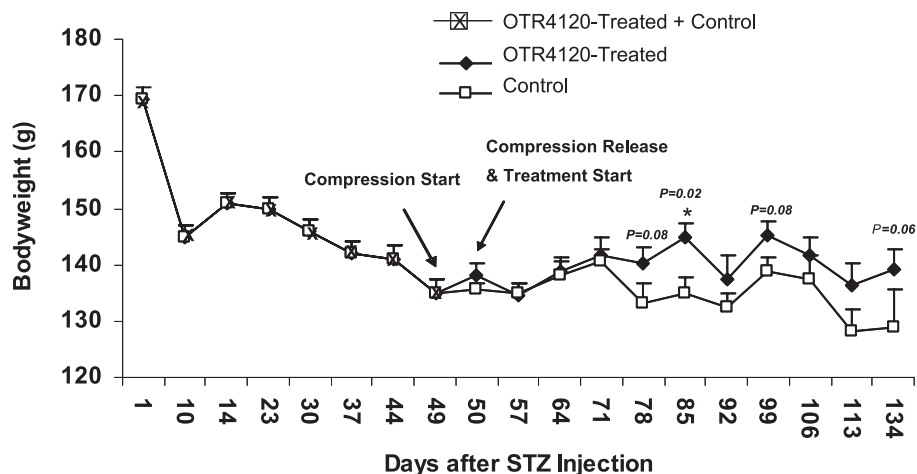


**FIG. 1.** Body weight measurement during diabetes induction (i.e., days 1–49 after STZ injection), ulceration, and ulcer healing (i.e., days 49–134). Data are presented as means  $\pm$  SEM. \**P* < 0.05 indicates significant difference in weight restoration after STZ injection between OTR4120-treated rats and control rats.

**Body weight changes.** During the diabetes induction period, the rats had a weight reduction of up to 17% (Fig. 1). After STZ injection, from 78 days onwards, the average weight restoration was, almost significantly, higher in the OTR4120-treated rats than in control rats (87 vs. 80% on day 78,  $P = 0.08$ ; 90 vs. 81% on day 85,  $P = 0.02$ ; 91 vs. 83% on day 99,  $P = 0.08$ ; and 87 vs. 77% on day 134,  $P = 0.06$ ) (Fig. 1).

**OTR4120 treatment reduced the degree of ulceration.** OTR4120-treated ulcers had significantly lower National Pressure Ulcer Advisory Panel grades compared with control ulcers on day 14 ( $1.68 \pm 0.23$  vs.  $2.50 \pm 0.25$ ,  $P < 0.05$ ).

**OTR4120 treatment accelerated ulcer healing.** Figure 2 shows that 90% of OTR4120-treated ulcers were completely closed on day 23 after compression release, compared with 50% of control ulcers ( $P < 0.05$ ). All OTR4120-treated ulcers were completely closed on day 42, whereas 14% of control ulcers were still open ( $P < 0.05$ ). All control ulcers were completely closed on day 49.

**OTR4120 treatment reduced neutrophil infiltration and stimulated inflammation resolution.** MPO activity was 28% lower in the OTR4120-treated rats compared with control rats on day 3 ( $P < 0.01$ ), and 48% lower on day 7

( $P < 0.05$ ) (Fig. 3). CD68 staining was detectable during the entire observation period. However, significantly reduced CD68 staining was found in OTR4120-treated ulcers on days 7, 14, and 84 (Fig. 4).

**OTR4120 treatment-enhanced angiogenesis.** The density score of CD34 staining in OTR4120-treated ulcers was significantly higher than in controls on day 14 ( $3.85 \pm 0.22$  vs.  $2.94 \pm 0.21$ ,  $P < 0.01$ ) and on day 42 ( $2.99 \pm 0.14$  vs.  $2.41 \pm 0.16$ ,  $P < 0.01$ ) (Fig. 5). The presence of VEGF was 197% higher in OTR4120-treated ulcers than in controls on day 14 ( $P < 0.05$ ) (Fig. 6A and D). TGF- $\beta$ 1 was 72% higher in OTR4120-treated ulcers than in controls on day 3 ( $P < 0.01$ ) and 40% higher on day 14 ( $P < 0.01$ ) (Fig. 6B and E). All scores had reduced to control levels on day 84.

**OTR4120 treatment revealed more iNOS.** In OTR4120-treated ulcers, the presence of iNOS was 66% higher on day 3 ( $4.04 \pm 0.46$  vs.  $2.43 \pm 0.52$ ,  $P < 0.05$ ) and 88% higher on day 14 ( $5.40 \pm 0.87$  vs.  $2.87 \pm 0.35$ ,  $P < 0.05$ ) compared with controls (Fig. 6C and F).

**OTR4120 treatment enhanced breaking strength.** The skin strength ratio in OTR4120-treated ulcers was 160% higher on day 18, 33% higher on day 42, and 33% higher on day 84 compared with controls (Fig. 7).

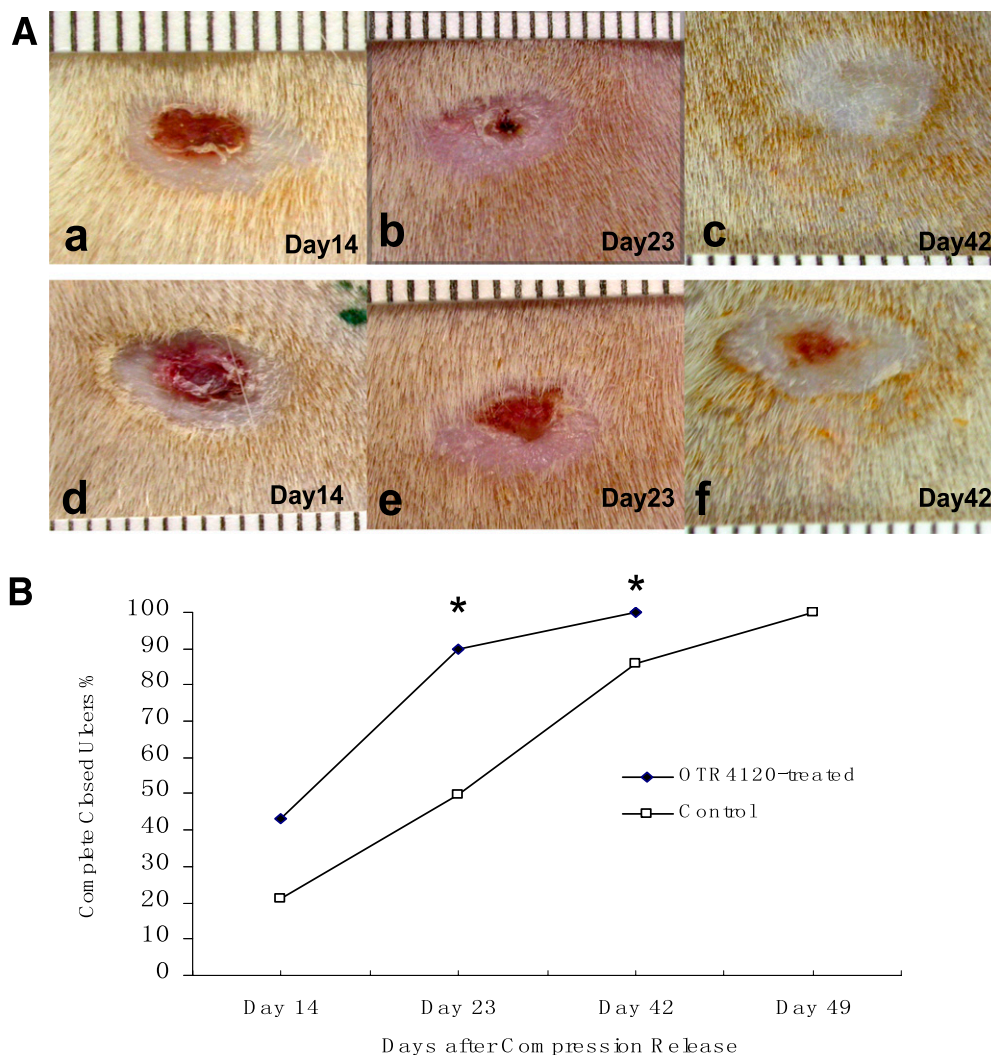


**FIG. 2.** Macroscopic evaluation of the ulcer healing time in OTR4120-treated and control rats. Representative photographs (A) of ulcers in OTR4120-treated rats on days 14 (a), 23 (b), and 42 (c) and in control rats on days 14 (d), 23 (e), and 42 (f). Percentage of complete closed ulcers (B). \* $P < 0.05$  indicates significant difference between the OTR4120-treated rats and control rats. (A high-quality color representation of this figure is available in the online issue.)

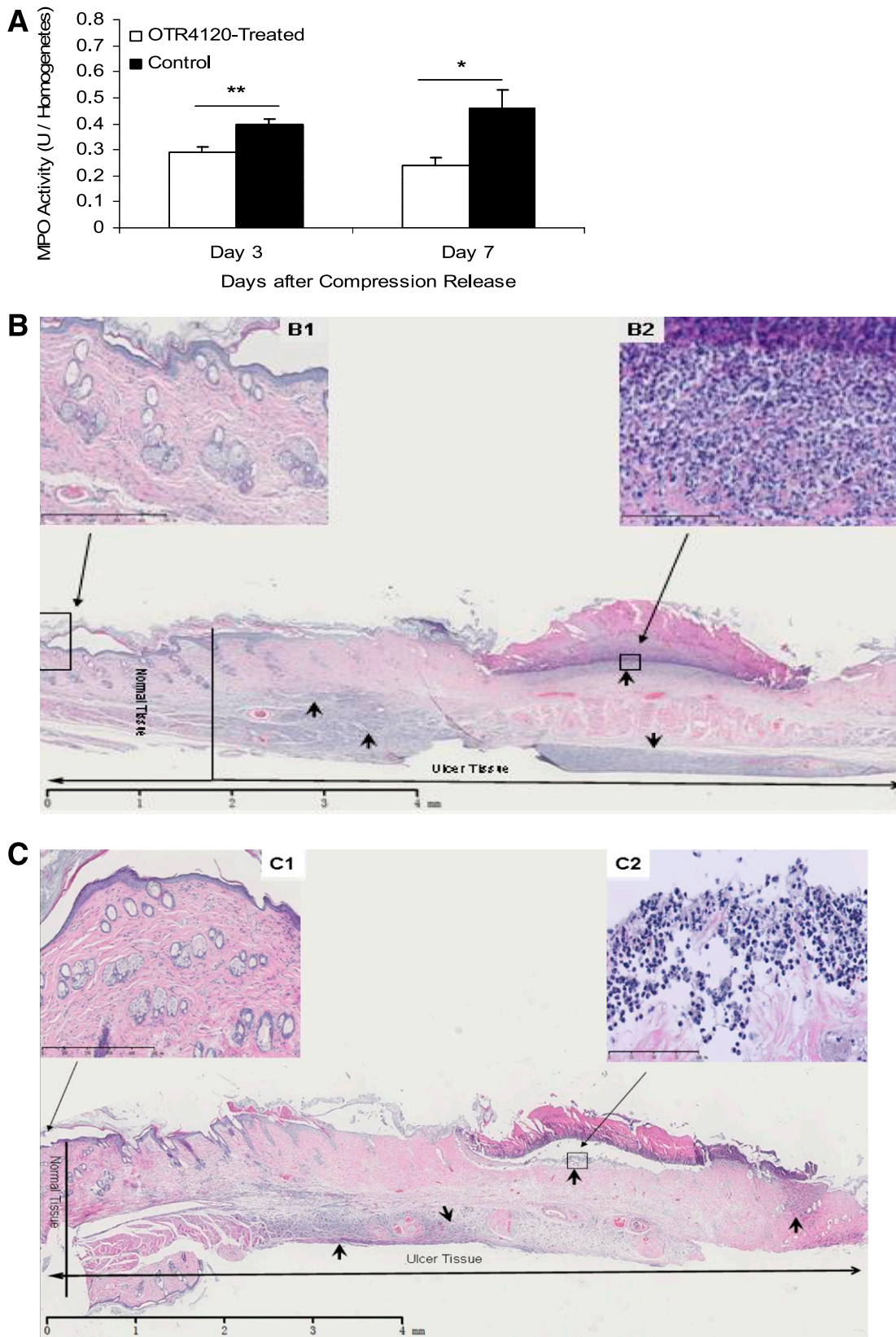


**FIG. 3.** Effect of OTR4120 treatment on reducing neutrophil infiltration assessed by MPO activity assay (A) and hematoxylin and eosin (H&E)-stained histology (B and C). Representative H&E staining section on day 7 after compression release of a control ulcer (B) shows intense infiltration of neutrophils (arrows) (original magnification  $\times 1.25$ ; scale bar = 4 mm) in the ulcer area, and an OTR4120-treated ulcer (C) shows less intense infiltration of neutrophils (arrows) (original magnification  $\times 1.25$ ; scale bar = 4 mm). B and C, top left insets: Normal skin tissue, located 2 mm from the ulcer margin of a control ulcer (B1) and an OTR4120-treated ulcer (C1) (original magnification  $\times 10$ ; scale bar = 500  $\mu\text{m}$ ). B and C, top right insets: Neutrophil infiltration at higher magnification of a control ulcer (B2) and an OTR4120-treated ulcer (C2) (original magnification  $\times 40$ ; scale bar = 100  $\mu\text{m}$ ). Data are presented as means  $\pm$  SEM. \* $P < 0.05$  and \*\* $P < 0.01$  indicate significant differences between the OTR4120-treated groups and control groups. (A high-quality color representation of this figure is available in the online issue.)

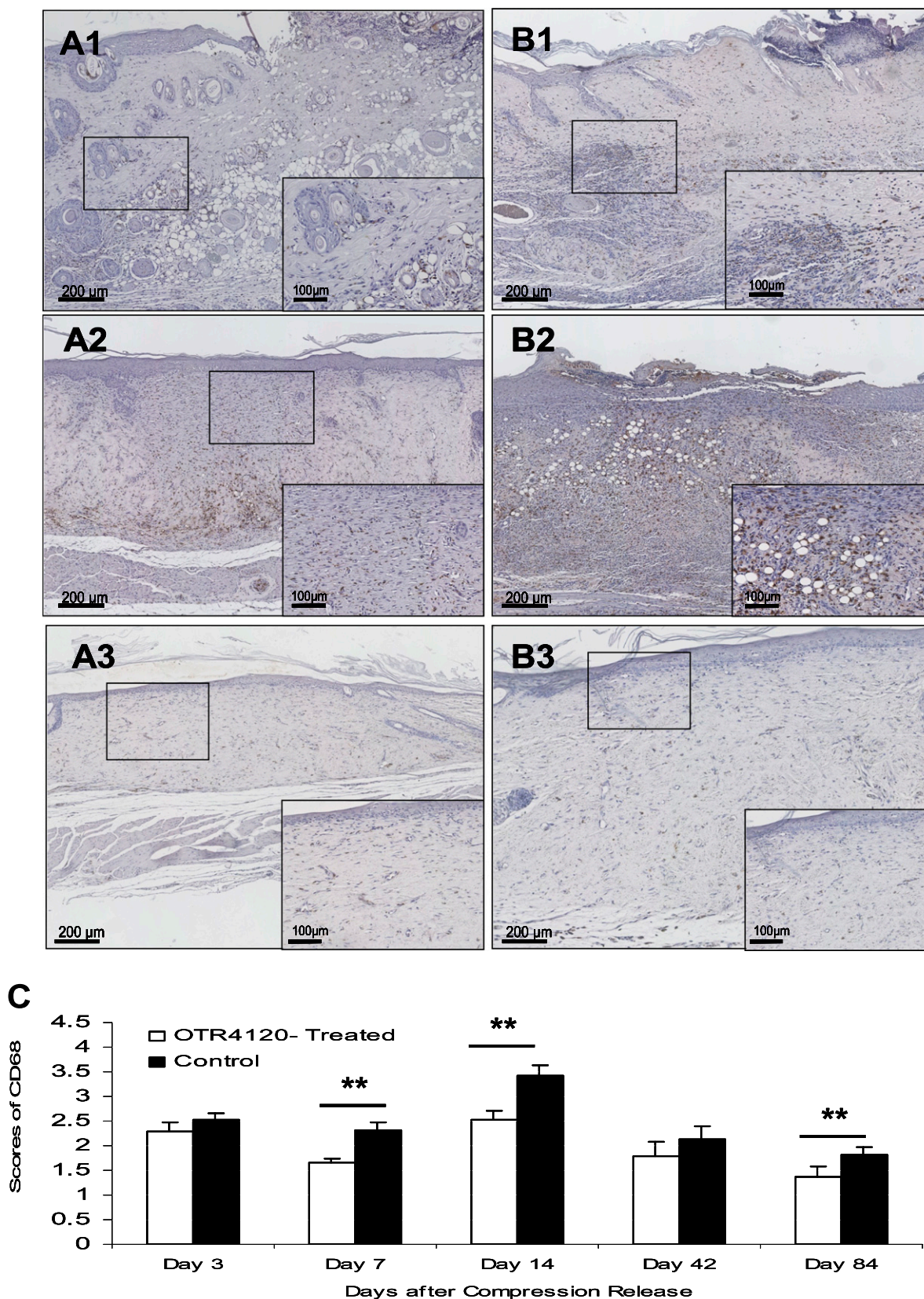
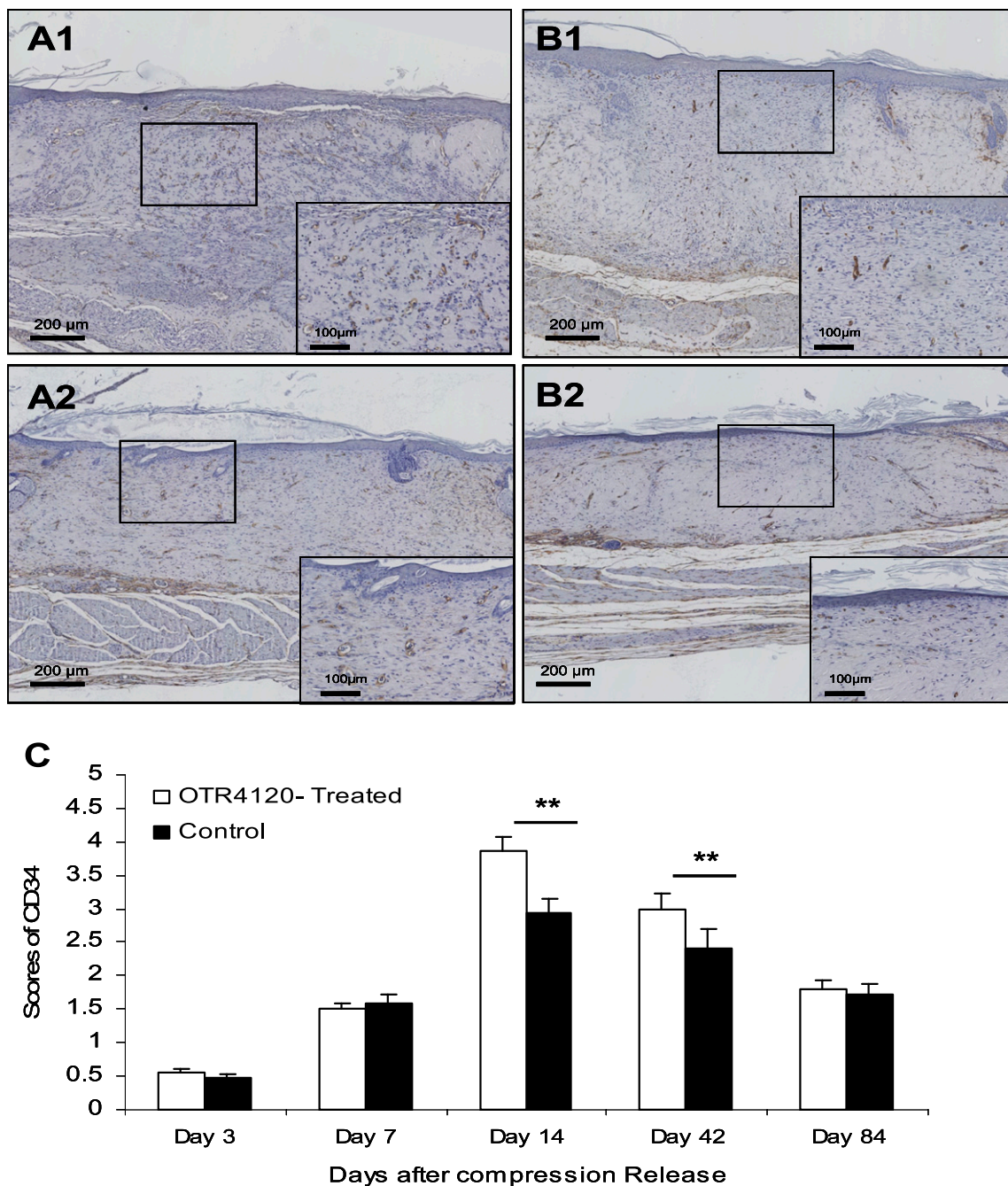


FIG. 4. Effect of OTR4120 treatment on inflammation reduction assessed by monocyte/macrophage marker CD68 immunohistochemistry. Representative CD68-staining sections of OTR4120-treated ulcers (A1–A3) and control ulcers (B1–B3) on days 7, 14, and 84 after compression release, respectively. Original magnification  $\times 40$ . Original inset magnification  $\times 200$ . Graphic visualization of scores of CD68 staining at indicated time points (C). Data are presented as means  $\pm$  SEM.  $**P < 0.01$  indicates significant difference between the OTR4120-treated groups and control groups. (A high-quality color representation of this figure is available in the online issue.)



**FIG. 5.** Effect of OTR4120 treatment on angiogenesis assessed by the endothelial cell marker CD34 immunohistochemistry. Representative CD34-staining sections of OTR4120-treated wounds (*A1* and *A2*) and control wounds (*B1* and *B2*) on days 14 and 42 after compression release, respectively. Original magnification  $\times 40$ . Original inset magnification  $\times 200$ . Graphic visualization of scores of CD34 staining at indicated time points (*C*). Data are presented as means  $\pm$  SEM.  $**P < 0.01$  indicates significant difference between the OTR4120-treated groups and control groups. (A high-quality color representation of this figure is available in the online issue.)

#### OTR4120 treatment increased hydroxyproline content.

The hydroxyproline content was increased in OTR4120-treated ulcers compared with controls on day 7 ( $9.81 \pm 0.34$  vs.  $6.89 \pm 0.42$   $\mu\text{g}$  hydroxyproline/mg homogenate,  $P < 0.05$ ) and on day 42 ( $14.31 \pm 1.11$  vs.  $10.18 \pm 1.01$   $\mu\text{g}$  hydroxyproline/mg homogenate,  $P < 0.05$ ).

**OTR4120 treatment increased ex vivo biosynthesis of collagen type I and reduced collagen type III.** The percentage of synthesized type I collagen was significantly increased in OTR4120-treated ulcers on day 42 ( $92.1 \pm 1.36$  vs.  $86.9 \pm 1.57$ ,  $P < 0.05$ ) (Fig. 8A). In contrast, type III

collagen synthesis was reduced in OTR4120-treated ulcers on days 7 and 42 ( $9.1 \pm 1.00$  vs.  $12.4 \pm 1.10$  on day 7,  $P = 0.07$ ;  $4.86 \pm 1.26$  vs.  $9.75 \pm 1.47$  on day 42,  $P < 0.05$ ) (Fig. 8B). The ratio of collagen type I to type III in the OTR4120-treated ulcers was increased twofold compared with control ulcers on day 42 ( $32.8 \pm 7.43$  vs.  $11.57 \pm 3.07$ ,  $P < 0.05$ ) (Fig. 8C).

**OTR4120 treatment had no effect on VEGF-A, TGF- $\beta$ 1, and iNOS gene transcription.** No statistical differences in VEGF-A, TGF- $\beta$ 1, and iNOS gene transcription were found between OTR4120-treated and control groups.

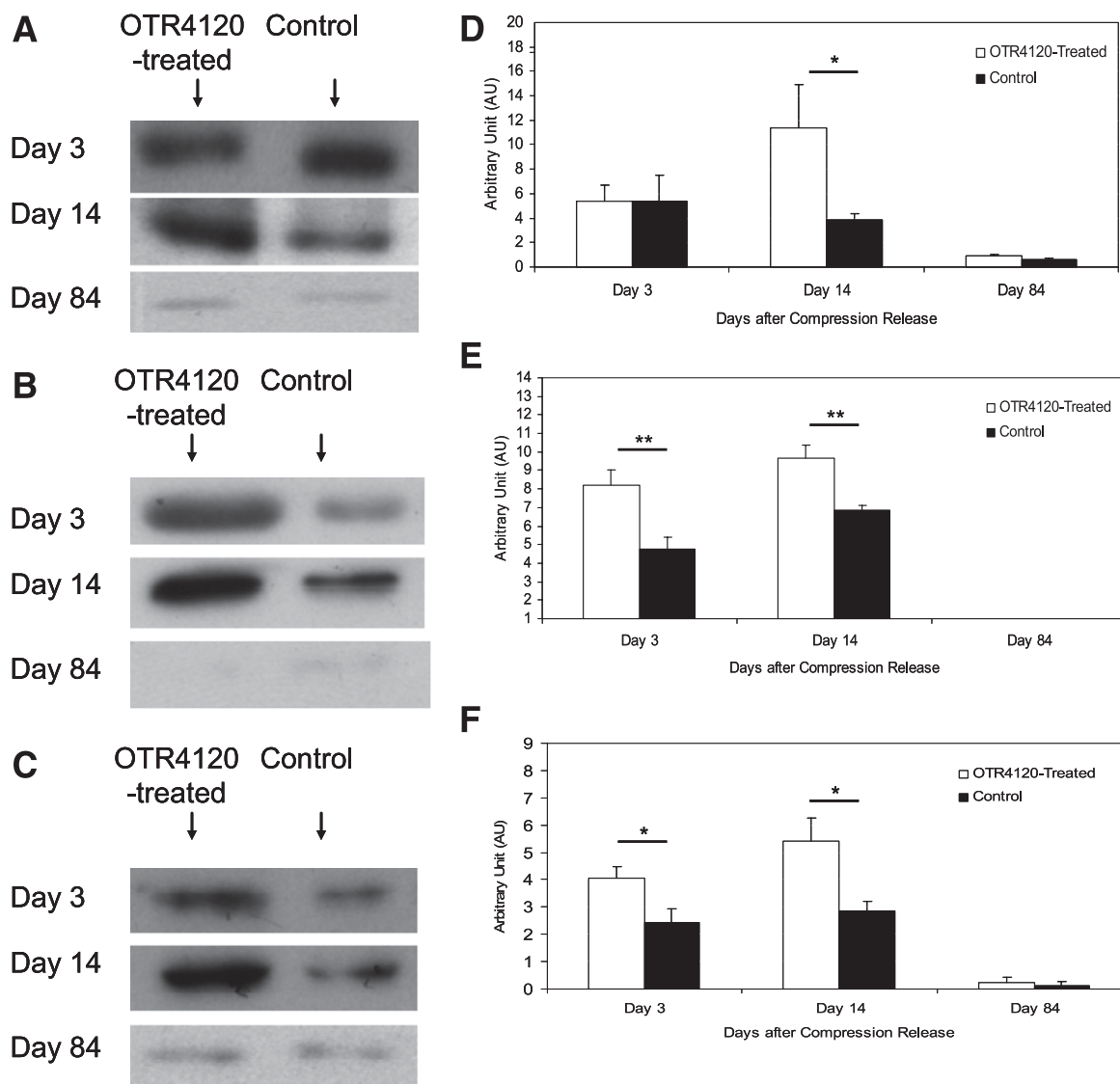


**FIG. 6.** Effect of OTR4120 treatment on VEGF, TGF- $\beta$ 1, and iNOS protein contents as assessed by Western blot analysis. Representative bands of VEGF (A), TGF- $\beta$ 1 (B), and iNOS (C) on days 3, 14, and 84 after compression release, respectively. Quantification of the VEGF (D), TGF- $\beta$ 1 (E), and iNOS bands (F). Data are presented as means  $\pm$  SEM. \* $P$  < 0.05 and \*\* $P$  < 0.01 indicate significant differences between the OTR4120-treated rats and control rats.

## DISCUSSION

Matrix therapy aims to facilitate and potentiate the intrinsic tissue self-regeneration capability by restoring the natural wound microenvironment. In this study, we demonstrate that matrix therapy with OTR4120 reduces diabetic ulcer healing time and improves healing quality by reducing inflammation, increasing angiogenesis, reducing collagen type III, enhancing the ulcer biomechanical strength restoration.

Excess inflammation, associated with a prolonged persistence of neutrophil infiltration, is a consistent feature of diabetes-impaired wound healing (6). In another study using the same wound model in normal rats, macrophages were only detectable during the first 6 weeks after wounding (14), whereas in the current study, macrophages were detectable during the entire 12-week observation period. This is an additional sign that inflammation resolution in diabetic wound healing is impaired. This impaired resolution is stimulated after OTR4120 treatment. Possible mechanisms of the anti-inflammatory properties of OTR4120 might

include its effect on inhibiting plasmin and neutrophil elastase activity (19,20) and increasing the content of TGF- $\beta$ 1 and VEGF that is demonstrated in this study. VEGF is known to induce macrophage apoptosis through stimulation of a tumor necrosis factor (21). The observed increase of TGF- $\beta$ 1 and VEGF in wounds of OTR4120-treated animals without an OTR4120 effect on TGF- $\beta$ 1 and VEGF gene transcription further strengthens their sequestering/protecting/stabilizing role on GFs.

Increased amounts of collagen type III relative to type I are often associated with excessive scarring during tissue remodeling (22). Ex vivo radiolabeling of collagen allowed us to compare the relative rates of biosynthesis of different collagen types that are thought to reflect collagen synthesis in the wounds directly before sampling. We observed that OTR4120 treatment reduced collagen type III synthesis and increased collagen type I synthesis in the late stages of wound healing. The antifibrotic effects of OTR4120 have been reported in healing Crohn disease intestinal biopsies (23) and burned rat skin (12). This effect is consistent with

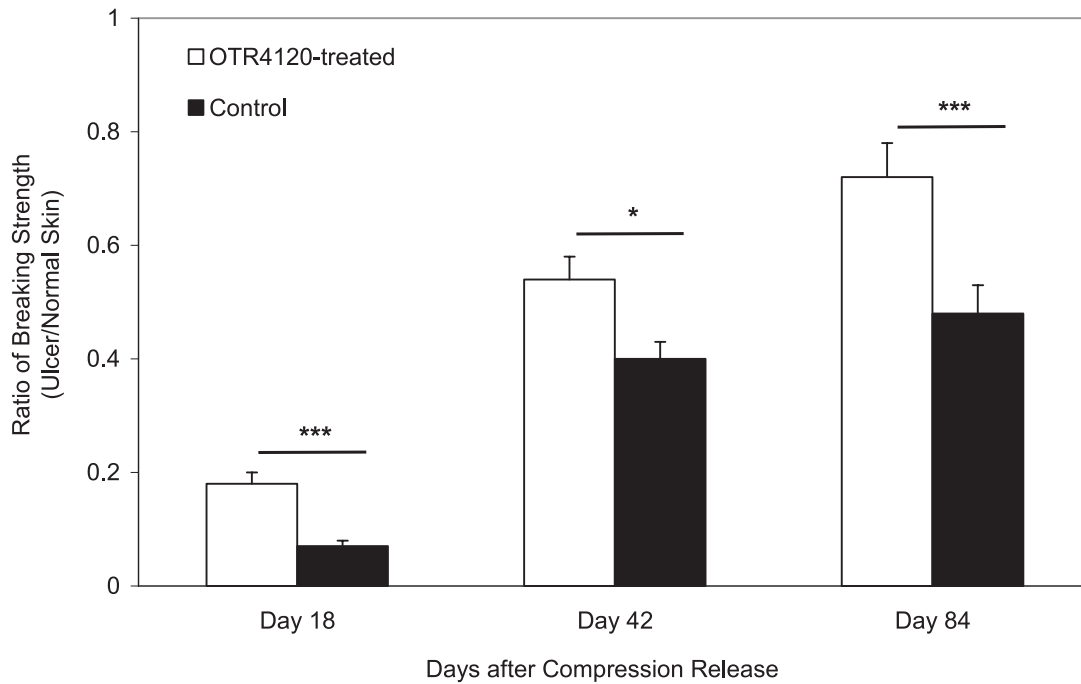


FIG. 7. Ratio of the wound-breaking strength of ulcer tissue compared with normal skin tissue on days 18, 42, and 84, respectively. Data are presented as means  $\pm$  SEM. \*\*\* $P < 0.001$ , \*\* $P < 0.01$ , and \* $P < 0.05$  indicate significant differences between treated and control groups.

the increased ulcer breaking strength after OTR4120 treatment. However, the underlying mechanisms of OTR4120 in regulating the relative proportion of collagen type I and type III during matrix remodeling remain unclear.

In addition to the anti-inflammatory and antifibrotic effects of OTR4120, this treatment also induced NO production. The diffusible, gaseous molecule NO participates in the orchestration of wound healing by modulating cytokines that are involved in wound healing (24). NO deficiency is an important mechanism for diabetes-impaired wound healing (24,25). Most cell types associated with wound healing are capable of producing NO through the activity of NOS. iNOS is calcium independent and controlled by inflammatory cytokines. Once iNOS has induced the production of NO, the content of NO within tissues can increase  $>1,000$ -fold (25).

The above data showed that OTR4120 treatment revealed a positive effect on wound healing. The enhanced wound healing is often an indicator of satisfactory nutritional status and weight gain. The weight restoration was found to be near-significantly improved after OTR4120 treatment. This improved weight gain may contribute to the regenerating effects of OTR4120 treatment on ulcer healing.

In summary, this study shows that a synthetic HS-GAG mimetic OTR4120 accelerates and improves diabetic pressure ulcer healing in rats. It suggests that OTR4120 treatment may be a promising matrix therapy for diabetes-impaired wounds.

#### ACKNOWLEDGMENTS

This research was supported by a grant from the Nuts Ohra Foundation (the Netherlands).

No potential conflicts of interest relevant to this article were reported.

M.T. researched data and wrote the manuscript. B.T. and J.W.v.N. researched data and edited the immunohistochemistry images. P.S., I.M.H., E.M.G.F., and M.G. researched data. S.E.R.H. contributed to the discussion. J.W.v.N. is the guarantor of this work and, as such, had full access to all the data

in the study and takes responsibility for the integrity of the data and the accuracy of the data analysis.

Parts of this study were presented in abstract form at the 14th European Conference of Scientists and Plastic Surgeons, Pamplona, Spain, 28–29 October 2011.

The authors thank Dr. V. Barbier and Dr. P. Kern (Laboratoire de Recherches sur la Croissance Cellulaire, Université Paris XII, Créteil, France) for their help in collagen biosynthesis measurements and OTR3 (Paris, France) for providing OTR4120.

#### REFERENCES

- Lioupis C. Effects of diabetes mellitus on wound healing: an update. *J Wound Care* 2005;14:84–86
- Maruyama K, Asai J, Ii M, Thorne T, Losordo DW, D'Amore PA. Decreased macrophage number and activation lead to reduced lymphatic vessel formation and contribute to impaired diabetic wound healing. *Am J Pathol* 2007;170:1178–1191
- Galiano RD, Tepper OM, Pelo CR, et al. Topical vascular endothelial growth factor accelerates diabetic wound healing through increased angiogenesis and by mobilizing and recruiting bone marrow-derived cells. *Am J Pathol* 2004;164:1935–1947
- Lobmann R, Ambrosch A, Schultz G, Waldmann K, Schiweck S, Lehnert H. Expression of matrix-metalloproteinases and their inhibitors in the wounds of diabetic and non-diabetic patients. *Diabetologia* 2002;45:1011–1016
- Schultz GS, Wysocki A. Interactions between extracellular matrix and growth factors in wound healing. *Wound Repair Regen* 2009;17:153–162
- Eming SA, Krieg T, Davidson JM. Inflammation in wound repair: molecular and cellular mechanisms. *J Invest Dermatol* 2007;127:514–525
- Menke NB, Ward KR, Witten TM, Bonchev DG, Diegelmann RF. Impaired wound healing. *Clin Dermatol* 2007;25:19–25
- Rouet Y, Hamma-Kourbali E, Petit P, Panagopoulou P, Katsoris D, Barritault J-P, Caruelle P, and J. Courty J. A synthetic glycosaminoglycan mimetic binds vascular endothelial growth factor and modulates angiogenesis. *J Biol Chem* 2005;280:32792–32800
- Rouet V, Meddahi-Pellé A, Maio HQ, Vlodayvsky I, Caruelle JP, and Barritault D. Heparin-like synthetic polymers, named RGTAs, mimic biological effects of heparin in vitro. *J Biomed Mater Res A* 2006;78:792–797
- Barritault D and Caruelle JP. [Regenerating agents (RGTAs): a new therapeutic approach]. *Ann Pharm Fr* 2006;64:135–144



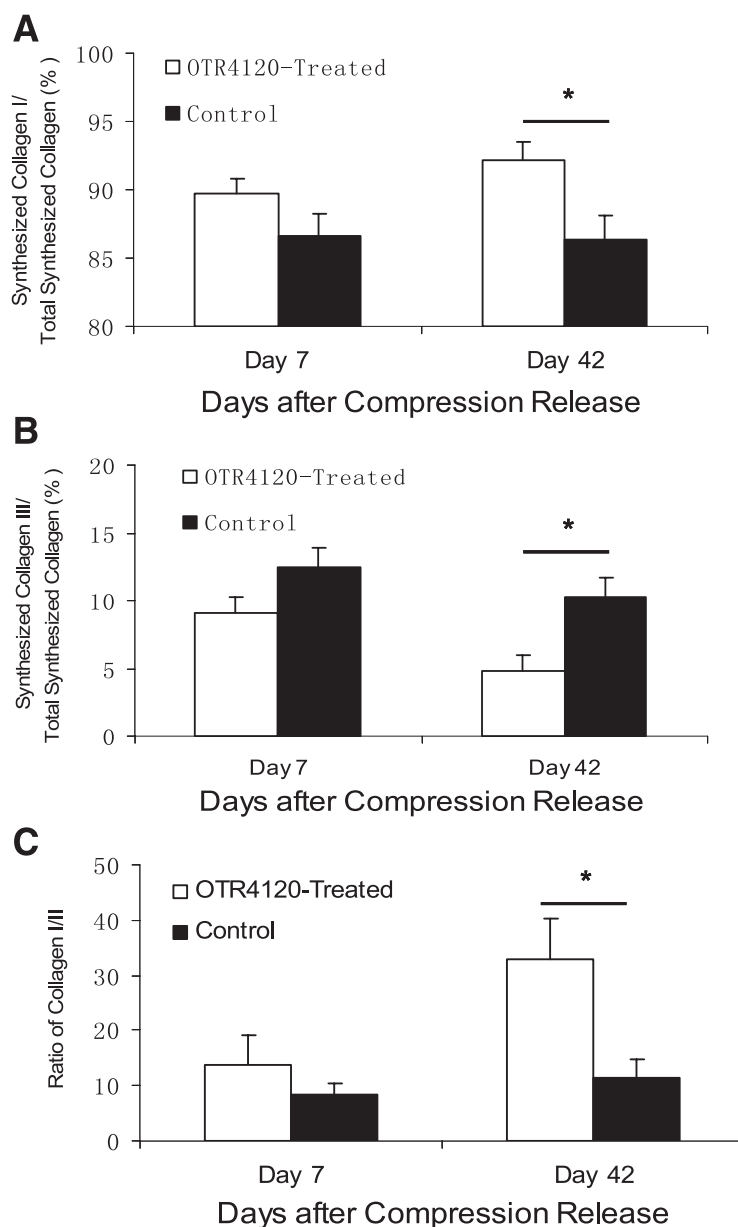


**FIG. 8. Biosynthesis of collagen type I and type III in ulcer tissue in control and OTR4120-treated rats.** Ulcer tissue samples were *ex vivo* labeled with [ $^3\text{H}$ ]hydroxyproline and digested by pepsin. Pepsin-soluble collagen types I and III were determined by SDS-PAGE. **A:** The percentage of synthesized collagen type I to total synthesized collagen. **B:** The percentage of synthesized collagen type III to total synthesized collagen. **C:** The ratio of collagen type I/collagen type III. Data are presented as means  $\pm$  SEM. \* $P < 0.05$  indicates significant difference between treated and control groups.

- Tong M, Tuk B, Hekking IM, Vermeij M, Barritault D, van Neck JW. Stimulated neovascularization, inflammation resolution and collagen maturation in healing rat cutaneous wounds by a heparan sulfate glycosaminoglycan mimetic, OTR4120. *Wound Repair Regen* 2009;17:840–852
- Garcia-Filipe S, Barbier-Chassefiere V, Alexakis C, et al. RGTA OTR4120, a heparan sulfate mimetic, is a possible long-term active agent to heal burned skin. *J Biomed Mater Res A* 2007;80:75–84
- Tong M, Zbinden MM, Hekking LJ, Vermeij M, Barritault D, van Neck JW. RGTA OTR 4120, a heparan sulfate proteoglycan mimetic, increases wound breaking strength and vasodilatory capability in healing rat full-thickness excisional wounds. *Wound Repair Regen* 2008;16:294–299
- Tong M, Tuk B, Hekking IM, et al. Heparan sulfate glycosaminoglycan mimetic improves pressure ulcer healing in a rat model of cutaneous ischemia-reperfusion injury. *Wound Repair Regen* 2011;19:505–514
- Zuijendorp HM, Smit X, Blok JH, Caruelle JP, Barritault D, Hovius SE, van Neck JW. Significant reduction in neural adhesions after administration of the regenerating agent OTR4120, a synthetic glycosaminoglycan mimetic, after peripheral nerve injury in rats. *J Neurosurg* 2008;109:967–973
- Lardenoye JW, Thiéfaïne JA, Breslau PJ. Assessment of incidence, cause, and consequences of pressure ulcers to evaluate quality of provided care. *Dermatol Surg* 2009;35:1797–1803
- Stark JM, van Egmond AW, Zimmerman JJ, Carabell SK, Tosi MF. Detection of enhanced neutrophil adhesion to parainfluenza-infected airway epithelial cells using a modified myeloperoxidase assay in a microtiter format. *J Virol Methods* 1992;40:225–242
- Woessner JF Jr. The determination of hydroxyproline in tissue and protein samples containing small proportions of this imino acid. *Arch Biochem Biophys* 1961;93:440–447
- Ledoux D, Papy-Garcia D, Escartin Q, et al. Human plasmin enzymatic activity is inhibited by chemically modified dextrans. *J Biol Chem* 2000;275:29383–29390
- Meddahi A, Lemdjabar H, Caruelle JP, Barritault D, Hornebeck W. FGF protection and inhibition of human neutrophil elastase by carboxymethyl

- benzylamide sulfonate dextran derivatives. *Int J Biol Macromol* 1996;18:141–145
21. Petreaca ML, Yao M, Ware C, Martins-Green MM. Vascular endothelial growth factor promotes macrophage apoptosis through stimulation of tumor necrosis factor superfamily member 14 (TNFSF14/LIGHT). *Wound Repair Regen* 2008;16:602–614
  22. Widgerow AD. Cellular/extracellular matrix cross-talk in scar evolution and control. *Wound Repair Regen* 2011;19:117–133
  23. Alexakis C, Caruelle JP, Sezeur A, et al. Reversal of abnormal collagen production in Crohn's disease intestinal biopsies treated with regenerating agents. *Gut* 2004;53:85–90
  24. Schwenker A, Vodovotz Y, Weller R, Billiar TR. Nitric oxide and wound repair: role of cytokines? *Nitric Oxide* 2002;7:1–10
  25. Boykin JV Jr. Wound nitric oxide bioactivity: a promising diagnostic indicator for diabetic foot ulcer management. *J Wound Ostomy Continence Nurs* 2010;37:25–32; quiz 33–34